Clim. Past Discuss., 11, 2889–2931, 2015
www.clim-past-discuss.net/11/2889/2015/
doi:10.5194/cpd-11-2889-2015

Climate of the Past Discussions
Open Access

A massive input of coarse-grained siliciclastics in the Pyrenean Basin during the PETM: the missing ingredient of a coeval abrupt change in hydrological regime

V. Pujalte[1], **J. I. Baceta**[1], **and B. Schmitz**[2]

[1]Dpt. of Stratigraphy and Paleontology, Faculty of Science and Technology, University of the Basque Country UPV/EHU, Ap. 644, 48080 Bilbao, Spain
[2]Division of Nuclear Physics, Department of Physics, University of Lund, P.O. Box 118, 221 00 Lund, Sweden

Received: 29 May 2015 – Accepted: 08 June 2015 – Published: 08 July 2015

Correspondence to: V. Pujalte (victoriano.pujalte@ehu.eus)

Published by Copernicus Publications on behalf of the European Geosciences Union.

Abstract

The Paleocene–Eocene thermal maximum (PETM) is represented in numerous shallow and deep marine sections of the south-central and western Pyrenees by a 2–4 m thick unit (locally ca. 20 m) of clays or marly clays intercalated within a carbonate-dominated succession. The massive input of fine-grained terrestrial siliciclastics into the Pyrenean Gulf recorded by that unit has been attributed to an abrupt hydrological change during the PETM. However, the nature of such change remains controversial. Here we show that, in addition to fine-grained deposits, large volumes of coarse-grained siliciclastics were brought into the basin that were mostly accumulated in incised valleys and a long-lived deep-sea channel, both spatially restricted settings. The occurrence of these coarse-grained deposits had been known for some time, but their correlation with the PETM is reported here for the first time. The bulk of incised valley PETM deposits are cross-bedded sands and pebbly sands, almost exclusively made of quartz, currently being actively quarried. Proof of their belonging to the PETM include: (1) their stratigraphic position, sandwiched between upper Thanetian and lower Ilerdian marine carbonates, (2) organic carbon isotope data, and (3) the fact that clay minerals from the sand matrix are more than 80 % kaolinite. The axially-flowing deep-sea channel existed throughout Paleocene times in the Pyrenean Basin, within which coarse-grained calciclastic turbidites, and lesser volumes of siliciclastic turbidites, were accumulated. This Paleocene succession is capped by thick-bedded turbiditic quartz sandstones and pebbly sandstones, here assigned to the PETM based on calcareous nannoplankton, clay mineral and organic carbon isotopic data. The large and simultaneous increase in coarse- and fine-grained terrestrial siliciclastic material delivered to the Pyrenean Gulf is related to an increased intra-annual humidity gradient. During the PETM longer and drier summer seasons facilitated the erosion of landscapes, whereas a dramatic enhancement of precipitation extremes during the wet seasons led to intensified flood events with rivers carrying greater volumes of bed and suspended loads. This scenario argues against the possibility that PETM kaolinites indicate a coeval

CPD
11, 2889–2931, 2015

warm and humid climate in northern Spain. Instead, the erosion of thick Cretaceous lateritic profiles developed in the Hercinian basement is proposed here as the most likely alternative.

1 Introduction

Paleocene and lower Eocene rocks of a whole range of facies are amply outcropped in the Pyrenean area (Fig. 1). The succession is up to 300 m thick and mainly consists of limestones and dolomites in shallow marine settings, and of alternations of hemipelagic marls and marlstones in deep marine settings. In these carbonate-dominated settings, however, mapping by the Geological Surveys of Spain and of the Basque Country made it evident the occurrence of a comparatively thin but laterally extensive fine-grained siliciclastic unit (FSU) around the Paleocene–Eocene (P–E) interval (e.g., Ríos Aragüés et al., 1972; Garrote et al., 1991). Correlation of the FSU with the Paleocene–Eocene thermal maximum (PETM) was first unequivocally confirmed in the deep marine Zumaia section by Schmitz et al. (1997) and in the shallow marine Urrobi and Mintxate sections by Pujalte et al. (2003) (location of sections in Fig. 1).

The FSU is usually 2–4 m thick, exceptionally reaching ca. 20 m, and it consists predominantly of fine-grained calcareous mudstones, which are dark grey in fresh outcrops but may change to reddish colours in weathered outcrops. The mudstones are rich in kaolinite, which in the well-known Zumaia section constitutes up to 75 % of the clay mineral assemblage (Knox, 1998; Gawenda, 1999). Carbonate content of the FSU in shallow marine sections ranges from 20–45 %, the carbonate fraction being largely represented by tests of large foraminifers, notably lenticular *Nummulites* (Pujalte et al., 2003). Carbonate content of the FSU is much lower in deep marine sections (0–10 %), being partly represented by an impoverished assemblage of planktonic and benthonic foraminifera and calcareous nannofossils (Schmitz et al., 1997; Orue-Etxebarria et al., 2004; Alegret et al., 2009). Additionally, in some sections such as Ermua (location in Fig. 1), the FSU includes thin-bedded calcarenites with resedimented microfossils (Pu-

CPD
11, 2889–2931, 2015

jalte et al., 1994; Baceta, 1996; Schmitz et al., 2001). These data demonstrate that a massive influx of terrestrial fine-grained siliciclastics was delivered to the Pyrenean Gulf during the PETM, which diluted but not entirely suppressed the autochthonous carbonate accumulation.

It is generally agreed that this siliciclastic influx was due to an abrupt hydrological change on the Pyrenean Gulf during the PETM. The nature of such change, however, is controversial, some papers arguing in favour of intensified precipitation (e.g., Pujalte et al., 1998a; Adatte et al., 2000), others of increased aridity (e.g., Bolle et al., 1998; Schmitz et al., 2001). Bolle et al. (1998) argued that kaolinite from the Ermua section was brought from lower latitudes by oceanic currents while arid conditions prevailed in the adjacent coastal area. Schmitz et al. (2001) reasoned that the increase of terrigenous siliciclastic detritus to the basin was associated with decreased grain size, a fact considered to imply reduced hydrodynamic energy of freshwater into the ocean, and drier conditions. The proposal of Schmitz et al. (2001) was also based on a tentative correlation of the FSU with prominent evaporite deposits occurring in the continental Tremp area (Fig. 1). However, subsequent studies by Schmitz and Pujalte (2003, 2007) established a robust correlation of the FSU with units of the Tremp area indicative of an enhanced seasonal humidity-gradient during the PETM (i.e., Claret Conglomerate and the Yellowish Soils). These authors found that, analogous to projected future changes following the present increase in atmospheric CO_2, semiarid regions during the PETM experienced prolonged and intensified drought during the summer seasons, and an increase in the strength and frequency of storm events in the cooler parts of the year. This circumstance, possibly in combination with a low sea-level, led to a dramatic increase in erosion of the vegetation-barren landscape during PETM.

The purpose of this paper is to test whether there is additional evidence, based on studies in the western Pyrenees, for dramatic and abrupt changes in the hydrological regime during the PETM. The most important new finding is that massive volumes of coarse-grained quartz sands and pebbly sands, and not only fine-grained siliciclastics, were supplied to the Pyrenean Gulf during the thermal event. The coarse-grained sili-

CPD
11, 2889–2931, 2015

ciclastics were accumulated in incised valleys in the shallow setting, and in a broad deep-sea channel in the deep basin, the confined nature of both depositional environments explaining why the occurrence of these coarse-grained deposits has been previously largely overlooked. It will also be shown that kaolinite from the FSU was likely supplied from Cretaceous lateritic profiles developed in the adjacent Hercynian basament of N Spain.

2 Data set and methods

This paper is mainly based on new field and laboratory data from three areas of the western Pyrenees (boxes 1, 2 and 3 in Fig. 1). Field data include mapping of these areas and logging and sampling of the P–E interval of selected sections. Laboratory data comprise analyses of carbon isotopes, mainly from dispersed organic matter ($\delta^{13}C_{org}$) but a few also from carbonate nodules ($\delta^{13}C_{inorg}$), clay mineralogy, and petrological study of thin sections. The organic carbon ^{13}C / ^{12}C analyses were carried out at the Servizos de Apoio á Investigación (SAI) of the University of A Coruña, Spain. Samples were weighed in silver capsules, decarbonated using 25 % HCl, and measured by continuous flow isotope ratio mass spectrometry using a MAT253 mass spectrometer (ThermoFinnigan) coupled to an elemental analyser EA1108 (Carlo Erba Instruments) through a Conflo III interface (ThermoFinnigan). Carbon stable isotope abundance is expressed as $\delta^{13}C$ (‰) relative to VPDB. International reference standards (NBS-22, IAEA-CH-6 and USGS 24) were used for $\delta^{13}C$ calibration. Replicate analyses were carried out on some of the decarbonated samples, which revealed negligible mean standard deviations.

Fine-grained samples were analyzed for their mineralogical content by X-ray diffraction (XRD) using a PANalytical Xpert PRO diffractometer at SGIker X-ray Facility of the University of the Basque Country, Spain. Samples were mechanically ground to powder in order to determine their general mineralogy in randomly oriented samples. For

CPD
11, 2889–2931, 2015

analysis of clay minerals, samples were decarbonated using diluted HCl and the suspension obtained was centrifuged until removal of chlorides. The < 2 µm fraction was separated by centrifugation, and oriented aggregates of this fraction were analyzed by XRD following three steps: first, air-dried without any additional treatment; second, after ethylene glycol solvation for 48 h at room temperature, in order to identify smectite; and, third, after dimethyl sulphoxide solvation at 75 °C for 72 h, in order to identify kaolinite and chlorite. Semiquantitative abundances were assessed using the intensity (area) of the major XRD reflections and applying the corresponding correction factors.

This paper also makes use of stratigraphical, palaeontological and palaeogeographical data of lower Palaeogene deposits of the Pyrenean area obtained in previous studies. However, these data were previously scattered in various publications, mainly two field guides (Pujalte et al., 1994; Baceta et al., 2011) and a PhD Thesis (Baceta, 1996), and are presented here in a coherent manner for the first time.

3 General setting

Throughout early Paleogene times the Pyrenean domain was an E–W elongated marine embayment opening into the Bay of Biscay, with a central deep-water trough (Basque Basin) flanked by a broad shallow marine carbonate platform, in turn surrounded by subaerial coastal alluvial plains (Fig. 1; Plaziat, 1981; Baceta, 1996; Baceta et al., 2011). The alluvial plain in the Tremp area was fed with calciclastic deposits derived from Cretaceous carbonate rocks uplifted during a Santonian–early Maastrichtian tectonic phase in the eastern Pyrenees. In addition, the Massif Central in France and the Ebro Massif in Spain, both made of Palaeozoic and lower Triassic rocks, supplied siliciclastic sediments (Fig. 1). The carbonate platform is mainly represented by a stack up to 300 m thick of shallow-marine carbonates, which can be broadly subdivided into inner and outer platform domains based on their fossil content and their respective dolomite/limestone proportions (Fig. 1). Significant amounts of sands and sandstones also occur, which were mostly accumulated within valleys incised in the

CPD
11, 2889–2931, 2015

inner platform domain (Baceta et al., 1994). The base-of-slope apron, typified by the Ermua section, is made up variable proportion of carbonate breccias, coarse-grained and fine-grained calciturbidites and hemipelagic limestones and marls (Pujalte et al., 1994, 1998b; Schmitz et al., 2001). These largely resedimented accumulations fringe the carbonate platform, from which they were clearly shed. The deep-marine Basque Basin, which is situated down current from the base-of-slope apron, is much more widespread (Fig. 1). It accumulated a rhythmic alternation of hemipelagic limestones and marls with minor intercalations of thin-bedded turbidites, exemplified by the well-known Zumaia section (Baceta, 1996; Pujalte et al., 1998b; Dinarès-Turell et al., 2003, 2007; Bernaola et al., 2006; Schmitz et al., 2011). The deep-sea channel is a long-lived, axially-flowing erosional feature that offers many clues for a correct understanding of the sedimentation processes in the Basque Basin during Paleocene times. Scattered outcrops of deep-sea channel deposits can be found from Pau, in the North Pyrenean zone, to Bilbao, in the westernmost tip of the Biscay synclinorium (Fig. 1; Pujalte et al., 1994; Baceta, 1996). This paper focuses on two of these sedimentary environments, the incised fluvial valleys and the deep-sea channel, discussing the architecture and facies of their deposits across the P–E interval.

4 The P–E interval in the inner platform domain

The P–E interval is represented in the inner platform domain of the south-western Pyrenees by two different kinds of successions. One of them, typified by the Korres section, is mostly comprised of shallow marine carbonates, and represents areas outside the incised valleys (Figs. 2, 3). Valley fill successions, of which the Laminoria section is the most representative, are characterized by the presence of massive volumes of siliciclastic sediments, notably sands and pebbly sands of fluviatile origin, which as a rule overlie an erosion surface deeply carved into upper Thanetian marine carbonates (Fig. 3). Mapping demonstrates that valley fill successions are laterally discontinuous,

CPD
11, 2889–2931, 2015

the orientation of the valleys having been reconstructed using palaeocurrents (Baceta et al., 1994; Fig. 2b).

Two incised valleys have been recognized, respectively situated to the southeast and to the west of the city of Vitoria (Figs. 1 and 2a). Their best outcrops occur in the Laminoria and Villalain quarries, the valleys being therefore named after them. A width of ca. 6 km can be estimated for the Laminoria valley (Fig. 2b). Width of the Villalain valley was probably similar, although outcrop constrains preclude its accurate reconstruction. Elsewhere in the southern Pyrenees lower Palaeogene inner platform outcrops are either eroded or buried under younger deposits (Fig. 1), which prevents establishing whether or not additional valleys existed.

4.1 Description of key sections

4.1.1 Korres section

The Korres section (42°41′55″ N, 2°26′11″ W), which is situated about 1 km east of the extrapolated eastern margin of the Laminoria incised valleys (Fig. 2), exemplifies a lower Palaeogene succession of the inner platform domain (Pujalte et al., 1994; Baceta, 1996). The Thanetian–lower Ilerdian interval is there represented by deposits of two different depositional sequences separated by an important discontinuity (DS TH-2 and DS IL-1; Baceta et al., 2011). Both are rich in marine microfossils, including several diagnostic larger foraminifera species (Fig. 3; fossil determination by Serra-Kiel, in Pujalte et al., 1994), based on which the two depositional sequences can be respectively ascribed to the Shallow Bentic Zone (SBZ) 4, late Thanetian, and SBZ-5, early Ilerdian (= earliest Ypresian) of Serra-Kiel et al. (1998).

Depositional sequence TH-2 rests abruptly on lower Thanetian recrystallized limestones and dolomitic marls and consists of two lithological units (A and B in Fig. 3). Unit A (ca. 10 m) is made up of an alternation of cross-bedded sandy limestones and sandy marls. Unit B (ca. 20 m) consists of thickly bedded grainstones and sandy grainstones rich in algal remains and larger foraminifera, and it is capped by a sharp surface

CPD
11, 2889–2931, 2015

of irregular morphology caused by a dense array of sub-vertical down-tapering pipes up to 20 cm in diameter and no less than 1 m deep (Figs. 3 and 4a, b). The pipes are filled with sandy calcarenites, similar in composition to the encasing bedrocks, but which include numerous hardened coated grains, which give the pipe fills a distinctive rugged appearance in weathered surfaces (Fig. 4c). Diameters of these coated grains vary between 2 and 35 mm, the smaller ones being typically spherical, the large ones ovoidal in shape (Fig. 3d). They have large nuclei and thin cortices. The nuclei are formed of quartz grains and lithoclasts set in a micritic matrix, the thin cortices by vaguely laminated micrite with irregularly developed circungranular cracks (Fig. 4e).

Vertical to subvertical pipes with coated grains similar to that from the Korres section were described in recent soils of Tarragona, Spain, by Calvet and Julià (1983, their Fig. 1b) and in the British West Indies by Jones (2011, his Fig. 2a), who respectively named them pisoids and oncoids. In both cases the pipes were developed in exposed Miocene carbonates, the coated grains occurring around roots of trees and bushes penetrating the rocky substratum. Based on that, it is safely to conclude that the irregular discontinuity capping unit B at Korres represents a surface of subaerial exposure colonized by plants.

The DS IL-1 sequence also has two lithological units at Korres (F and G in Fig. 3). Unit F is ca. 7 m thick, and it is made up of calcareous clays devoid of fossils but containing scattered and small-sized (< 3 mm) soil carbonate nodules, indicative of poorly developed soils. The overlying unit G corresponds to the so-called *Alveolina* limestone, a laterally extensive marine unit of the Pyrenees recording a basin-wide, early Eocene transgression (e.g., Plaziat, 1975; Baceta et al., 2011; Pujalte et al., 2014a). In the Korres section, unit G is at least 20 m thick (top not preserved) and it is mostly composed of sandy calcarenites rich in shallow marine fauna, dominated by flosculinized alveolinids (Fig. 3).

CPD
11, 2889–2931, 2015

4.1.2 Laminoria and Villalain sections

The incised valley successions are accessible in four quarries (Fig. 2), two of which are currently active, Laminoria (42°46′45″ N, 2°28′00″ W) and Villalain (42°54′43″ N, 3°35′19″ W). In these quarries the DS TH-2 is only represented by unit A, which is truncated at its top by an erosional unconformity, the inherent hiatus involving the removal of, at least, 21 m of the sequence (Figs. 3 and 5a). By contrast, the DS IL-1 includes three lithological units not present in the Korres section or elsewhere outside the valleys (units C, D and E in Fig. 3).

Unit C is poorly outcropped, not being of economic interest and therefore not quarried (Fig. 5a). Exploratory shallow boreholes demonstrate that it is up to 7 m thick (J. R. Subijana, personal communication, 2015). In its scattered outcrops the unit is mostly composed of red unfossiliferous clays with subordinate interbedded sand lenses. Neither carbonate nodules nor carbonate-coated rizocretions have been observed in the clays, only occasional root traces less than 1 mm in diameter. The sandstone lenses vary in thickness from 0.5 to 4 cm, exhibiting cross-laminations, sharp bases and undulating tops.They consist mainly of very fine to fine quartz grains cemented by calcite. The lower and upper surfaces of many of the lenses are coated with mm-thick crusts of hematite and goethite (Fig. 4a, inset).

Unit D, the main objective of the quarrying, is up to 10.5 m thick and mainly composed of fine-medium quartz sands (diameters 0.1–0.7 mm), mostly used in moulds for foundries and for quality glass. The sands may contain up to 20 % of clay matrix, more than 80 % of which is kaolinite. Other minor components are pebbles and heavy minerals, which are respectively separated from the target quartz sands by sieving and wet spiral concentrators (J. R. Subijana, personal communication, 2015). Pebbles occur randomly dispersed in the sands (Fig. 5b). They range 1–10 cm in diameter, most being subrounded fragments of white or pink vein quartz, but clasts of quartzite and quartzarenites also occur. In the active front of the quarries the sands have light brownish colours, but in the inactive Arenaza quarry (location in Fig. 2) ex-

CPD
11, 2889–2931, 2015

hibit a superficial reddish colour (Supplement Fig. 2a). Also in this inactive quarry, the top 10–15 cm of the sands are intensely impregnated by hematite (Supplement Fig. 2b and c). Some of the bigger clasts exhibit distinctive polished flattened facets of ventifacts (Fig. 5c). These, at least, must have been ultimately derived from Permian rocks, where ventifacts are comparatively frequent, and which are not uncommonly resedimented into younger formations (Segura and Elorza, 2013). Neither body fossils nor trace fossils have been observed, although hematite-coated root casts occur at some levels (Fig. 5e). Metre-thick sets bounded by internal erosional surfaces can be seen at Laminoria and Villalain (Fig. 5d and f). The bounding surfaces have a concave-up shape in the former quarry, which is oriented almost at right angles to the palaeocurrents, and near flat in the Villalain quarry, oriented approximately parallel to the palaeocurrents. Further, unidirectional cross-stratification with decimetre to metre scale foresets can be clearly perceived at Villalain (Fig. 5f). These geometries are indicative of large-scale unidirectional trough cross-bedding, a type of bedding amply described in fluviatile deposits (e.g., Allen, 1983; Bridge, 2003). The absence of marine body fossils or trace fossils, and the occasional occurrence of root casts, support the fluviatile interpretation.

Unit E is up to 4 m thick and caps the incised valley succession in both the Laminoria and Villalain quarries (Figs. 3 and 5d, f). At Laminoria it can be subdivided in two parts (E1 and E2 in Figs. 3 and 5d). Part E1 (3 m) mainly consists of silts with a few intercalated sand beds 5–10 cm thick. At Laminoria at least two horizons crowded with vertical root casts coated with iron oxides can be seen (Figs. 3 and 5e). At Villalain part E1 is not represented. As a rule, unit E2 is sharply overlain by the *Alveolina* limestone unit G, the abrupt lower boundary of which in all probability represents a ravinement surface recording the Ilerdian transgression.

4.2 Age model for the Laminoria and Korres clastic units

It is now firmly established that the PETM took place around the SBZ4/SBZ5 (or Thanetian/Ilerdian) boundary (e.g., Orue-Etxebarria et al., 2001; Pujalte et al., 2003, 2009;

CPD
11, 2889–2931, 2015

Scheibner et al., 2005; Zamagni, 2012; Drobne, 2014). The clastic units C, D, E and F of Laminoria and Korres are all intercalated between SBZ4/SBZ5 marine deposits and, consequently, it is reasonable to assume that at least some of them may be coeval with the thermal event. To test this possibility thirteen samples from the Laminoria sections were analyzed for organic carbon isotopes, and nine samples for clay mineralogy (Fig. 6a). Routine analyses of the clay matrix of the sands of unit D always produce a high kaolinite content (80–100 %; J. R. Subijana, personal communication, 2015). In addition, four samples from the Korres section were analyzed for isotopes and one for clay mineralogy, the results being shown in Fig. 6b, and discussed below.

A pulse of kaolinite accumulation in connection with the PETM has been documented on widely separated sections of the North Atlantic, such as Zumaia on the Bay of Bicay, northern Spain (Knox, 1998; Gawenda et al., 1999) and the Bass River on the New Jersey margin, USA east coast (Gibson et al., 2000; John et al., 2012). At Zumaia kaolinites first appear in significant amounts (up to 25 % of the clay mineral assemblage) some 10 m below the onset of the PETM, the proportion increasing sharply (up to 75 %) at the onset of the thermal event (Knox, 1998). The origin of the pulse is controversial (e.g., John et al., 2012) but, together with carbon isotope data, it is here used to establish and age model for clastic units C–F.

The highest content in kaolinite occurs in unit D at Laminoria, which is accordingly tentatively ascribed to the core of the PETM. Only one clay sample for isotopic analysis could be collected from this unit, its isotopic value (−26.7 ‰ $\delta^{13}C_{org}$) being fully compatible with that proposal (Fig. 6a). Indeed, analyses of well-constrained P–E continental and marine sections elsewhere in the Pyrenees concur in that the PETM interval is characterized by $\delta^{13}C_{org}$ isotopic values ranging from −26.0 to −28.8 ‰, while pre- and post-PETM background values vary between −22.0 and −25.0 ‰ (e.g. Storme et al., 2012; Manners et al., 2013; Pujalte et al., 2014a).

In the same section the proportion of kaolinite in unit E decreases upward, in parallel with a steady trend towards less negative $\delta^{13}C_{org}$ values (Fig. 6a). Both sets of data are

CPD
11, 2889–2931, 2015

strongly indicative that unit E was accumulated, totally or in part, during the recovery phase of the PETM, further reinforcing the ascription of unit D to the PETM.

Dating of unit C is less well constrained, mainly because no fresh samples suitable for isotopic analyses could be obtained. However, a pre-PETM age is suggested by its stratigraphic position below unit D, and also by the comparatively low amount of kaolinite in the six samples analyzed (Fig. 6a).

Three additional significant data have been obtained from the Korres section (Fig. 6b): (1) the pisoids enclosed in the pipes at the top of unit B provide very negative $\delta^{13}C_{org}$ isotopic values (−26.1 and −28.1 ‰), (2) kaolinite is absent in the overlying unit F, its clay assemblage being 100 % illite, and (3) the carbonate soil nodules in the same unit give comparatively light $\delta^{13}C_{inorg}$ isotopic values (−5.1 and −5.8 ‰). According to these data the karstic surface at the top of unit B was created during the PETM, while unit F postdate the PETM.

4.3 Creation, evolution and filling of the incised valleys

It is widely acknowledged that the excavation of incised valleys in marine basin margins is usually triggered by a relative sea-level fall, the surface of subaerial exposure capping unit B at Korres confirming that scenario. Incised valleys are filled with sediments during the subsequent sea-level rise (e.g., Boyd et al., 2006; Strong and Paola, 2008).

Field data indicate that the sea-level drop trigering the incision of the Laminoria and Villalain valleys occurred during the latest Thanetian, prior to the onset of the PETM, and that the sea-level rise started before the thermal event, with deposition of unit C, and continued during and after it. Filling of the valleys occurred in three phases, respectively recorded by units C, D and E (Figs. 3 and 6a). These three units are considered of continental origin, based on the absence of fossils and the presence of root casts, but their contrasting lithologies and sedimentary features are indicative of very different depositional conditions.

Unit C must have been accumulated in a low energy setting, probably a flood plain, as demonstrated by the predominance of clays, the intercalated rippled sandstone lenses

CPD
11, 2889–2931, 2015

probably corresponding to distal crevasse splay deposits. Flood plains are best developed in meandering river systems. Therefore we speculate that point bar channel sands also exist in unit C, although none has been observed in the few available outcrops of the unit. The red colour of the clays suggests well-drained and oxidized soils, the absence of calcite either suggesting that their moisture was too high for calcite accumulation or that accumulations of the clays was too rapid for nodules to form.

The sedimentary feaures of unit D implies a drastic change in depositional conditions during the PETM. Indeed, the prevalence of sands and pebbly sands and the large-scale trough cross-bedding require a much greater stream power, and therefore water supply, than in the underlying unit C. Further, the scarcity of fine-grained deposits coupled with the large-scale trough cross-bedding or channelling in the pebbly sands clearly indicate a braided river system stretching across most, if not all, the width of the incised valleys.

The vertical reduction in grain size in unit E may denote a decrease in the river discharge, but more likely it records the backstepping and ponding of the fluvial system as the sea level rose. The widespread hematite-coated root traces in subunit E1, which suggest wet soil conditions, and the preservation of abundant coal remains in subunit E2 indicative of a waterlogged environment, are both fully compatible with that scenario. The eventual marine flooding of the valleys is demonstrated by the overlying *Alveolina* limestones of unit G (Fig. 5d and f). Field data, and the age model discussed above, further indicates a small time lag in the re-establishment of fully marine conditions outside the valleys (Fig. 3).

5 Paleocene deposits in the deep-water Basque Basin

The Paleocene Epoch is represented in the Basque Basin by two contrasting and mutually exclusive groups of deposits, hemipelagic and resedimented. Hemipelagic deposits occur in the central part of the deep basin and are represented by cyclic vertical alternations of marls and limestones, with minor alternations of thin-bedded turbidites. They

CPD
11, 2889–2931, 2015

have been the objective of intensive study, particularly in the Zumaia section but also in other coastal sections such as Sopelana, Hendaia or Bidart (Fig. 1), the papers resulting from these studies being too numerous to list here (e.g., Dinarès-Turell et al., 2014; Storme et al., 2014; Clare et al., 2015; Hilgen et al., 2015, to name but some recent publications). The hemipelagic Zumaia section is also the Global Stratotype Sections and Points for the Selandian and Thanetian Stages (Schmitz et al., 2011).

Resedimented deposits can in turn be subdivided in two groups. One group is mainly composed of clasts- and mud-supported carbonate breccias and thickly-bedded calciclastic turbidites. As recognized by Plaziat (1975, his Fig. 13), they were clearly shed from the shallow carbonate platform and were accumulated in the base-of-slope carbonate apron fringing it (Fig. 1). The Ermua section is representative of this type of accumulation (Pujalte et al., 1994; Baceta, 1996; Schmitz et al., 2001).

The second group of resedimented deposits include massive volumes of siliciclastic turbidites, in addition to clasts- and mud-supported carbonate breccias and thickly-bedded calciclastic turbidites (Figs. 7–11). These deposits, which occur in the axial part of the Basque Basin and provide many clues to properly understand its Paleocene and early Eocene palaeogeography and evolution, were until recently largely overlooked and sometimes misinterpreted. Thus, although their existence near Orio (location in Figs. 1 and 7) was reported more than sixty years ago (Gómez de Llarena, 1954), only two papers about them were produced in the following 28 years (Hanisch and Flug, 1974; van Vliet, 1982). In the former paper the resedimented deposits were considered a diapiric mass outflowed during the Cretaceous from the nearby Zarautz diapir (Fig. 7b). The latter paper provided a correct dating of the succession with calcareous nannoplankton (Fig. 7a and Supplement Fig. 1), but the only interpretation offered was that "this area [near Orio] remains stratigraphically anomalous until the earliest Eocene, as it also contains a localized very coarse-grained submarine fan body in the basal *Tribrachiatus contortus* zone (NP 10)" (van Vliet, 1982, pp. 32). As explained below, later studies by Pujalte et al. (1994) and Baceta (1996) made it evident that the

CPD
11, 2889–2931, 2015

second group of resedimented deposits were accumulate at the bottom of an axially flowing deep-sea channel (Fig. 1).

5.1 The deep-sea channel: architecture and evolution

Deep-sea channels are erosional submarine features deeply incised into unconsolidated sediment of ocean margin troughs or oceanic abyssal plains (Carter, 1988, p. 42). The realization that the Paleocene coarse-grained resedimented deposits of the axial part of the Basque Basin were accumulated on the floor of a deep-sea channel was mainly based on the following facts:

1. They are not restricted to the Orio outcrop but are found from near Pau in the northern Pyrenees to near Bilbao in the westernmost available outcrops (Fig. 1).

2. Flute casts from the base of thick-bedded turbitites, both calciclastic and siliciclastic, systematically indicate westwards directed palaeocurrents. In the case of Orio, palaeocurrents demonstrate transport towards the Zarautz diapir, not away from it (Fig. 7b).

3. A high resolution mapping of the eastern flank of the Zarautz diapir demonstrated that it had little influence in the accumulation of Paleocene resedimented deposits (Baceta et al., 1991). Except at Orio, no Keuper diapirs occur in the vicinity of axial Paleocene resedimented deposits, a further proof that diapirism played little or no role in their accumulation.

4. The trend of the deep-sea channel was inferred from palaeocurrents, its cross-section through correlation of well-dated sections. As datum for correlation the lower/upper Maastrichtian, Cretaceous/Paleogene and calcareous nanoplankton NP10/NP11 boundaries were used (Figs. 7 and 9).

5. As a rule, the resedimented deposits rest directly onto Campanian-lower Maastrichtian flysch deposits, as exemplified by the Orio and Gonzugaria sections.

CPD
11, 2889–2931, 2015

The lowermost part of the resedimented deposits at the Orio section is represented by a chaotic breccia, which is considered a testimony of the carving of the deep-sea channel (Fig. 7c). This breccia is mainly formed by large contorted blocks of upper Maastrichtian reddish marls, but also includes some large clasts of Paleocene hemipelagic limestones of the P1a planktonic foraminifera zone of Wade et al. (2011). The breccia is overlain by thickly-bedded calciturbidites with thin marly interbeds containing well-preserved planktonic foraminifera of the P1c zone. These data indicate that creation of the channel was initiated in early Danian times.

The information summarized above and illustrated in Figs. 7–9 demonstrates that the Paleocene deep-sea channel was at least 200 km long, about 5 km wide and up to 350 m deep (i.e., the maximum thickness of the missing section at Orio and Gonzugaraia). The channel was carved into a succession ("pre-channel suite") in which two parts are recognized, the Campanian-lower Maastrichtian siliciclastic flysch and the upper Maastrichtian reddish marls and marly limestones. After the initial excavation of the channel during the early Danian, it persisted as a prominent geomorphological feature until the earliest Eocene. The channel had a dominantly erosive character, acting essentially as a conduit for concentrated turbidite currents. Outside the channel hemipelagic sedimentation was the rule. Consequently, three different types of Paleocene sedimentary successions ("syn-channel suite") are recognized in the Basque Basin: (1) Basin floor association, typified by the Zumaia section, which is largely made up of a continuous stack of hemipelagic limestones and marls. (2) Channel-wall association, lithologically similar to the previous one, but getting thinner and with increasingly important internal hiatuses towards the channel axis. The Balcón de Bizkaia, and Trabakua pass west section are representative of this association (Fig. 9). (3) Channel-bottom association, mostly composed of coarse-grained resedimented deposits, with thin and discontinuous intercalations of hemipelagic marls. The lower part of this association is dominated by thickly-bedded calciturbidites intermingled with intraformational breccias derived from the slumps and collapses of the channel walls, while the upper part is dominated by thickly-bedded siliciclastic turbidites (Figs. 8 and 10a).

CPD
11, 2889–2931, 2015

The deep-sea channel was created during an interval of comparative sediment starvation in the Basque Basin and lasted, while starvation persisted, until the earliest Eocene. Sedimentation rates increased dramatically during the early Eocene and, in the comparatively short time of the NP10 zone (1.39 My according to Berggren et al., 2005), the deep-sea channel was filled up by the massive arrival of mixed calciclastic and siliciclastic turbidites ("post-channel suite", Figs. 7 and 9).

5.2 The PETM interval at the Orio section

Given the scarce attention hitherto received by the Paleocene resedimented deposits of the deep-sea channel it is hardly surprising that no attempt has been made to pinpoint in them the PETM. The Orio section was selected to alleviate this information deficit for several reasons. One, it is the thickest section of resedimented deposits available in the Basque Basin (Baceta, 1996). Two, its carbonate-dominated intervals are well dated with planktonic foraminifera and/or larger foraminifera and/or calcareous nannofossils (Fig. 7c, Supplement Fig. 1). Third, a recent enlargement of the road connecting the N-634 road to the E-5 motorway has created a fresh outcrop of the upper segment of the section, (the target of this study), from which fresh samples could be collected (Figs. 8d and 11a).

The target segment is situated above Thanetian calciturbidites and just below deposits of the post-channel suite that contain *Tibrachiatus contortus* (Supplement Fig. 1), a nannofossil species that post-dated the PETM (Aubry, 1996). The interval is exclusively made up of siliciclastic deposits, but two different parts can be readily differentiated (parts A and B in Figs. 8d and 11b). Part A is composed of plane-parallel turbidite beds separated by thin clay interbeds. The sandstones are medium-grained and loosely cemented, probably due to superficial decalcification. Thin sections reveal that, in addition to quartz, they contain around 5–7 % of feldspars and lesser amount of mica and rock fragment, and can thus be classified as subarkoses (Fig. 8d).

Part B is composed of amalgamated sandstones and pebbly sandstones, the latter with clasts up to 3 cm in diameter (Fig. 8f). They are thickly-bedded, beds ranging

CPD
11, 2889–2931, 2015

2–5 m in thickness. The sandstones are quartzarenites, composed of more than 95 % of quartz, with just traces of mica and rock fragments, and are pervasively cemented by quartz. Part B is therefore very resistant to erosion, creating a prominent ridge in the landscape (Fig. 8a and b). Some of the sandstone bed surfaces are strewn with coalified remains (Fig. 8e). The great thickness of the beds, their absence of grading or internal laminations and the occurrence of coalified remains of obvious continental derivations strongly suggest that most, if not all the sandstones of part B are hyperpycnal flow turbidites, generated by direct river effluent (cf., Plink-Björklund and Steel, 2004). Clay interbeds are rare, thin and discontinuous (Fig. 11b).

The stratigraphic position of the target segment suggests that it, or a part of it, may pertain to the PETM (Supplement Fig. 1). To test that possibility 13 samples were analyzed for organic carbon isotopes, 12 of them from clays or plant remains, the remainder from marls. Additionally, 6 samples were analyzed for clay mineralogy. Location of the samples and the analytical results are plotted in Fig. 11.

The four samples analyzed from part A give a stable isotopic trend, with $\delta^{13}C_{org}$ values in the range −24.2 to −24.4 ‰ (Fig. 11b). This is the same value range obtained from the uppermost Paleocene part of the Zumaia section by Storme et al. (2012) and, accordingly, a pre-PETM age is assigned to part A. Values from the eight samples analyzed from part B drop to around −27.6 to −28.4 ‰, typical $\delta^{13}C_{org}$ values of the PETM at Zumaia, again according to Storme et al. (2012). Consequently, part B is assigned to the PETM. This inference is further supported by the stratigraphical position of part B (Supplement Fig. 1) and by the $\delta^{13}C_{org}$ value of −24.8 ‰ obtained from one marly sample collected just above part B, which is indicative of the return to background conditions after the thermal event.

The three clay samples from part A analyzed for clay minerals exclusively contain illite, while two out of the three samples analyzed from part B include a significant percentage of kaolinite (Fig. 11b). Although somewhat ambiguous, the clay results do not contradict the age inferred from the isotope data.

CPD
11, 2889–2931, 2015

6 Discussion

The three main findings of this study are that: (1) in the western Pyrenees the PETM was preceded by a sea-level fall, recorded by the subaerial exposure of the inner marine carbonate platform and the excavation of incised valleys, (2) in connection with the thermal event, massive volumes of sands and pebbly sands were stored in the incised valleys and in the bottom of the deep-sea channel, (3) the influx of kaolinite during the PETM was especially important in the incised valleys.

A pre-PETM fall of sea level has previously been documented in the eastern Pyrenees (Pujalte et al., 2014a), in the North Sea Basin (Dupuis et al., 2011) and even in Egypt (Speijer and Morsi, 2002). The evidence here presented further reinforces that the fall was, at least, supraregional.

The PETM coarse-grained siliciclastics in the incised valleys and in the deep-sea channel are clear proof of a large increase in, respectively, stream power (which required greater discharges), and the flow strength and capacity of turbidite currents. Coarse-grained sands have also been documented in PETM deltas (Fig. 12a, Pujalte et al., 2014b). To evaluate the significance of such increases, however, it must be taken into account that the volume of fine-grained siliciclastics delivered to the Pyrenean Gulf during the PETM far exceeded that of sands and pebbly sands. As a result, a mud blanket on average 3 m thick covered most of the outer platform (Pujalte et al., 2003), the base-of-slope apron (Schmitz et al., 2001), the basin floor (Schmitz et al., 1997; Baceta, 1996) and, more remarkable, the deep-sea channel walls (Figs. 9b and 10b).

Two lines of reasoning converge to indicate that the most plausible explanation of the hydrological change in the Pyrenean Gulf during the PETM was an abrupt enhancement of seasonal precipitation extremes in an overall dry environment. One, models predict that the ongoing global warming will increase the frequency of interannual precipitation extremes, especially the wet extremes (e.g., Berg and Hall, 2015). Two, it is well established that in semi-arid areas interannual variation in precipitation rates are strong and that, during flood events, suspended sediment concentrations in rivers

CPD
11, 2889–2931, 2015

are very high. For example, data compiled from the semi-arid Carapelle watershed in southern Italy by Bisantino et al. (2011, their Table 3) show that the concentration of suspended sediments in the Carapelle torrent during intense flood events may be as high as 43 g L^{-1}. Even higher suspension load concentrations (250 g L^{-1}) during flood events have been measured in the Wadi Wahrane of Algeria (Benkhaled and Remini, 2003).

Semi-arid to arid climates prevailed during Palaeocene times in the Pyrenean Gulf, as demonstrated by paleosols rich in calcareous nodules and gypsum in the continental Tremp Group of the eastern Pyrenees (Schmitz and Pujalte, 2003). Accordingly, the rise in temperatures during the PETM, would prolong and intensify summer drought but increase the frequency and magnitude of cool-season flood events. This would increase the river channel competence and the volume of suspension loads.

The change in channel pattern recorded in the incised valleys, from meandering during accumulation of unit C to braided during accumulation of unit D (Fig. 12b), is congruent with the hydrological change proposed above. The possibility that this change was caused by a tectonic event is considered highly unlikely, since tectonic quiescence prevailed in the Pyrenean domain throughout the latest Maastrichtian–middle Ilerdian interval (e.g., Fernández et al., 2012; Pujalte et al., 2014a). Further, Bridge (2003) maintains that river channel patterns are determined by the type of flows at averaged bankfull discharges ("channel-forming discharges"), a configuration that is only slightly modified at low discharges. Bridge (2003, his Fig. 5.9) also indicates that the width/depth and degree of braiding of rivers increase as their channel-forming discharges increase. Thus, the observed change to a braided pattern can reasonably be attributed to the higher frequency and magnitude of flood events during the PETM.

Changes registered in the deep sea-channel can also be explained in the context of the PETM hydrological change. The deep-sea channel acted mainly as a conduit towards deeper water of turbidite currents reaching the central part of the Basque Basin. During most of Paleocene time these turbidites mainly carried coarse clastics, either carbonate or siliciciclastics, while channel-walls were subjected to erosion and

CPD
11, 2889–2931, 2015

the basin floor mainly received hemipelagic sediments (Fig. 12c). During the PETM interval field evidence demonstrates that hyperpycnal flow turbidites entering the deep-sea channel carried, in addition to coarse-grained sands and pebbly sands, an even larger fraction of fines in suspension that overflowed the channel bottom and were deposited on the channel walls an in the basin floor, greatly diluting the hemipelagic contribution (Fig. 12c).

The influx of kaolinite during the PETM has been reported in widely separated basins, although its origin is somewhat controversial (John et al., 2012). Kaolinites have been reported in several PETM sections of the Pyrenean Gulf in variable percentages, ranging from up to 15 % of the total clay assemblage in the continental Tremp Basin (Schmitz and Pujalte, 2003) to up to 75 % in the Zumaia section (Knox, 1998). Here we show that kaolinites occur at even higher percentages in unit D, within the incised valleys (Fig. 6a), which were probably sourced from the Hercinian Ebro Massif (Fig. 1). The Ebro Massif is currently buried by younger Tertiary sediments (Lanaja and Navarro, 1987). However, the Hercinian basement outcrops further south and it is amply documented that it was covered by a thick lateritic profile developed under tropical conditions during the Cretaceous, the remains of which may be more than 50 m thick (Molina Ballesteros, 1991). The remnants of this profile are directly overlain by a lower Palaeogene alluvial unit named “Siderolithic Series”, which at least in part was derived from the lateritic profile (Santisteban Navarro et al., 1991; Molina Ballesteros et al., 2007). The Siderolithic unit consists of channelized conglomerates and sandstones and overbank fines, their main components being quartz and kaolinite. Also significant, the conglomerates and sandstones are cemented by silica and by variable amounts of Fe oxyhydroxides, the latter giving the unit its name.

The quartz-rich character of unit D at Laminoria and Villalain, and its content on hematite and goethite strongly suggest that it resulted from the erosion of a similar Cretaceous lateritic profile developed on the Ebro Massif. Therefore, the high content in kaolinite of the unit can best be explained by enhanced erosion of this old profile, instead than recording intense chemical weathering under the greenhouse climate of the

CPD
11, 2889–2931, 2015

PETM. The variable content in kaolinite in the different PETM sections of the Pyrenees can thus be attributed to differences in the source areas, the highest and lowest fluxes being respectively derived from the Ebro Massif in the south and from the calcareous mountains in the east (Fig. 1), the intermediate values in the Basque Basque sections probably recording a mixed contribution from both source areas.

7 Conclusions

The important change in sedimentary conditions recorded in the western part of the Pyrenean Gulf across the P–E boundary interval can satisfactorily be explained by a dramatic and abrupt change in hydrology and a pre-PETM sea-level fall. During the PETM drier periods were longer and interval of intense rain more frequent. In a dry, vegetation-barren landscape seasonal precipitation extremes effectively eroded the landscape. As a result, during rainy intervals fluvial currents carried coarser bed loads and massive suspension loads. Delivering of these loads to the marine basin was facilitated by the lowering of the sea level. A fraction of the bed load was accumulated within incised valleys, excavated during the sea-level fall, and on deltas at the valley mouths. The remainder coarse-grained fraction, transported by hyperpycnal flows, reached a deep-sea channel excavated along the axial part of the Basque Basin. Distribution of the suspension load was much more widespread, its deposits covering much, if not all, the outer platform, the base-of-slope, the basin floor and even the walls of the deep-sea channel. This implies that the rivers transported and delivered a much larger volume of fine-grained sediments than of coarse-grained sediments, another indication of precipitation extremes. The evidence that the influx of kaolinite coeval with the PETM was due to enhanced erosion of Cretaceous lateritic profiles developed on the Hercinian basement reinforce this conclusion.

Based on an entirely different set of data from the Tremp–Graus Basin, in the eastern Pyrenees, a similar hydrological change to the one discussed here was proposed by Schmitz and Pujalte (2007). The data from the western Pyrenees here presented

CPD
11, 2889–2931, 2015

reinforce such a proposal, and indicate that the hydrological change affected the entire Pyrenean domain.

The Supplement related to this article is available online at doi:10.5194/cpd-11-2889-2015-supplement.

Acknowledgements. Funds to VP and JIB were provided by Research Project CLG2011-23770 (Ministerio de Economía y Competitividad, Spanish Government) and Research Group of the Basque University System, Basque Government, IT-631-13. Funds to BS were provided by the Swedish Research Council (LUCCI Linné Grant). The advise provided by Gilen Bernaola on the calcareous nannofossil data of van Vliet is greatly appreciated. We are grateful to María Lema Grille for the isotope analyses and Javier Sangüesa for the X-Ray analyses. Thanks are extended to Juan Echave and to Jose Ramón Subijana, owner and geologist of the sand quarries, for granting permission to visit and sampling the Laminoria and Villalain quarries, and for their information about the composition of the sands.

References

Adatte, T., Bolle, M. P., de Kaenel, E., Gawenda, P., Winkler, W., and von Salis, K.: Climatic evolution from Paleocene to earliest Eocene inferred from clay-minerals: a transect from northern Spain (Zumaya) to southern (Spain, Tunisia) and southeastern Tethys margins (Israel, Negev), GFF, 122, 7–8, 2000.

Alegret, L., Ortiz, S., Orue-Exteberria, X., Bernaola, G., Baceta, J. I., Monechi, S., Apellaniz, E., and Pujalte, V.: The Paleocene–Eocene thermal maximum: new data on microfossil turnover at the Zumaia section, Spain, Palaios, 24, 318–328, 2009.

Allen, J. R. L.: Studies in fluviatile sedimentation: bars, bar complexes and sandstone sheets (low-sinuosity braided strean) in the Brownstones (L. Devonian), Sedim. Geol., 33, 237–293, 1983.

Aubry, M. P.: Towards an upper Paleocene-lower Eocene high resolution stratigraphy, in: Paleocene/Eocene Boundary Events in Space and Time, edited by: Aubry, M. P. and Benjamini, C., Israel Journal of Earth Sciences, 44, 239–253, 1996.

CPD
11, 2889–2931, 2015

Baceta, J. I.: El Maastrichtiense superior, Paleoceno e Ilerdiense inferior de la Región Vasco-Cantábrica: secuencias deposicionales, facies y evolución paleogeográfica, PhD thesis, University of the Basque Country, 372 pp., 1996.

Baceta, J. I., Pujalte, V., Robles, S., and Orue-Etxebarria, X.: Influencia del diapiro de Zarautz sobre los procesos de resedimentación paleocenos de Orio (Guipúzcoa, Cuenca Vasca), Geogaceta, 9, 57–60, 1991.

Baceta, J. I., Pujalte, V., and Payros, A.: Rellenos de valles encajados en el Maastrichtiense superior y Paleógeno inferior de Alava (Plataforma Noribérica, Cuenca Vasca), Geogaceta, 16, 86–89, 1994.

Baceta, J. I., Pujalte, V., Serra-Kiel, J., Robador, A., and Orue-Etxebarria, X.: El Maastrichtiense final, Paleoceno e Ilerdiense inferior de la Cordillera Pirenaica, in: Geología de España, edited by: Vera, J. A., Sociedad Geológica de España-Instituto Geológico y Minero de España, Madrid, 308–313, 2004.

Baceta, J. I., Pujalte, V., Wright, V. P., and Schmitz, B.: Carbonate platform models, sea-level changes and extreme climatic events during the Paleocene-early Eocene greenhouse interval: a basin–platform–coastal plain transect across the southern Pyrenean basin, in: Pre-Meeting Field-Trips Guidebook, 28th IAS Meeting, Zaragoza, edited by: Arenas, C., Pomar, L., and Colombo, F., Sociedad Geológica de España, Geo-Guías, 7, 101–150, 2011.

Benkhaled, A. and Remini, B.: Temporal variability of sediment concentration and hysteresis phenomena in the Wadi Wahrane basin, Algeria, Hydrol. Sci. J., 48, 243–255, 2003.

Berg, N. and Hall, A.: Increased interannual precipitation extremes over california under climate change, J. Climate, in press, doi:10.1175/JCLI-D-14-00624.1, 2015.

Berggren, W. A., Kent, D. V., Swisher III, C. C., and Aubry, M. P.: A revised Cenozoic geochronology and chronostratigraphy, in: Geochronology, Time Scales and Global Stratigraphic Correlations, edited by: Berggren, W. A., Kent, D. V., Aubry, M. P., and Hardenbol, J., S. E. P. M. Spec. Publ., 54, 129–212, 1995.

Bernaola, G., Baceta, J. B., Payros, A., Orue-Etxebarria, X., and Apellaniz, E.: The Paleocene and lower Eocene of the Zumaia section (Basque Basin), in: Post-Conference fieldtrip Guidebook of the CBEP Meeting 2006, ISBN: 84-689-8940-1, 82 pp., 2006.

Bisantino, T., Gentile, F., and Liuzzi, G. T.: Continuous monitoring of suspended sediment load in semi-arid environments, in: Sediment Transport, edited by: Ginsberg, S. S., 295–312, 2011.

CPD
11, 2889–2931, 2015

Bolle, M. P., Adatte, T., Keller, G., von Salis, K., and Hunziker, J.: Biostratigraphy, mineralogy and geochemistry of the Trabakua Pass and Ermua sections in Spain, Ecolog. Geol. Helv., 91, 1–25, 1998.

Boyd, R., Dalrymple, R. W., and Zaitlin, B. A.: Estuarine and Incised-Valley Facies Models, in: Facies Models Revisited, edited by: Posamentier, H. W. and Walker, R. G., SEPM (Society for Sedimentary Geology) Sp. Pub., 84, 171–235, 2006.

Bridge, J. S.: Rivers and Flood Plains, Forms, Processes, and Sedimentary Record, Blackwell Publishing, 491 pp., 2003.

Calvet, F. and Julià, R.: Pisoids in the caliche profiles of Tarragona, north east Spain, in: Coated Grains, edited by: Peryt, T. M., Springer-Verlag, Berlin, 456–473, 1983.

Carter, R. M.: The nature and evolution of deep-sea channel systems, Basin Res., 1, 41–54, 1988.

Clare, M. A., Talling, P. J., and Hunt, J. E.: Implications of reduced turbidity current and landslide activity for the Initial Eocene Thermal Maximum – evidence from two distal, deep-water sites, Earth Planet. Sc. Lett., 420, 102–115, 2015.

Dinarès-Turell, J., Baceta, J. I., Pujalte, V., Orue-Etxebarria, X., Bernaola, G., and Lorito, S.: Untangling the Palaeocene climatic rhythm: an astronomically calibrated Early Palaeocene magnetostratigraphy and biostratigraphy at Zumaia (Basque basin, northern Spain), Earth Planet. Sc. Lett., 216, 483–500, 2003.

Dinarès-Turell, J., Baceta, J. I., Bernaola, G., Orue-Etxebarria, X., and Pujalte, V.: Closing the Mid-Palaeocene gap: toward a complete astronomically tuned Palaeocene Epoch and Selandian and Thanetian GSSPs at Zumaia (Basque Basin, W Pyrenees), Earth Planet. Sc. Lett., 262, 450–467, 2007.

Dinarès-Turell, J., Westerhold, T., Pujalte, V., Röhl, U., and Kroon, D.: Astronomical calibration of the Danian stage (Early Paleocene) revisited: settling chronologies of sedimentary records across the Atlantic and Pacific Oceans, Earth Planet. Sc. Lett., 405, 119–131, 2014.

Drobne, K., Jez, J., Cosovic, V., Ogorelec, B., Stenni, B., Zakrevskaya, E., and Hottinger, L.: Identification of the Palaeocene–Eocene Boundary based on Larger Foraminifers in deposits of the Palaeogene Adriatic Carbonate Platform, Southwestern, Slovenia, in: STRATI 2013, edited by: Rocha, R., Pais, J. Kullberg, J. C., and Finney, S., Springer International Publishing, Switzerland, 89–93, 2014.

Dupuis, C., Quesnel, F., Iakovleva, A., Storme J- Y., Yans, J., and Magioncalda, R.: Sea level changes in the Paleocene–Eocene interval in NW France: evidence of two major drops en-

CPD
11, 2889–2931, 2015

compassing the PETM, in: Climate and Biota of the Early Paleogene, Conference Program and Abstracts, Salzburg, Austria, edited by: Egger, H., Berichte der Geologischen Bundesanstalt, 85, p. 63, 2011.
Fernández, O., Muñoz, J. A., Arbués, P., and Falivene, O.: 3D structure and evolution of an oblique system of relaying folds: the Ainsa basin (Spanish Pyrenees), J. Geol. Soc. London, 169, 545–559, 2012.
Garrote, A., García-Portero, J., Fernández-Carrasco, J., Cerezo, A., Tijero, F., and Zapata, M.: Mapa Geológico del País Vasco a escala 1 : 25.000, Hoja 63-III, Eibar, Ente Vasco de la Energía, Bilbao, 1991.
Gawenda, P., Winkler, W., Schmitz, B., and Adatte, T.: Climate and bioproductivity control on carbonate turbidite sedimentation (Paleocene to earliest Eocene, Gulf of Biscay, Zumaia, Spain), J. Sediment. Res., 69, 1253–1261, 1999.
Gibson, T. G., Bybell, L. M., and Mason, D. B.: Stratigraphic and climatic implications of clay mineral changes around the Paleocene/Eocene boundary of the northeastern US margin, Sedim. Geol., 134, 65–92, 2000.
Gómez de Llarena, J.: Observaciones en el Flysch Cretácico-Nummulítico de Guipúzcoa, Monografías Inst. Lucas Mallada, 13, 1–98, 1954.
Hanisch, J. and and Flug, R.: The interstratified breccias and conglomerates in the Cretaceous Flysch of the northern Basque Pyrenees: submarine outflow of diapiric mass, Sedim. Geol., 12, 287–296, 1974.
Hilgen, F. J., Abels, H. A., Kuiper, K. F., Lourens, L. J., and Wolthers, M.: Towards a stable astronomical time scale for the Paleocene: aligning Shatsky Rise with the Zumaia–Walvis Ridge ODP Site 1262 composite, Newsletter on Stratigraphy, 48, 91–110, 2015.
John, C. M., Banerjee, N, R., Longstaffe, F. J., Sica, C., Law, K. R., and Zachos, J. C.: Clay assemblage and oxygen isotopic constraints on the weathering response to the Paleocene-Eocene thermal maximum, east coast of North America, Geology, 40, 591–594, 2002.
Jones, B.: Biogenicity of terrestrial oncoids formed in soil pockets, Cayman Brac, British West Indies, Sedim. Geol., 236, 95–108, 2011.
Knox, R. W. O. B.: Kaolinite influx within Palaeocene/Eocene bounday strata of western Europe (extended abstract), Newsletter on Stratigrahy, 36, 49–53, 1998.
Lanaja, J. M. and Navarro, A.: Contribución de la exploración petrolífera al conocimiento de la Geología de España, Instituto Geológico y Minero de España, Madrid, 465 pp. 1987.

CPD
11, 2889–2931, 2015

Manners, H. R., Grimes, S. T., Sutton, P. A., Domingo, L., Leng, M. J., Twitchett, R. J., Harta, M. B., Jones, T. D., Pancost, R. D., Duller, R., and López-Martínez, N.: Magnitude and profile of organic carbon isotope records from the Paleocene–Eocene Thermal Maximum: evidence from northern Spain, Earth Planet. Sc. Lett., 376, 220–230, 2013.

Molina Ballesteros, E.: Paleoalteraciones y evolución del relieve: el caso del Zócalo Hercínico Ibérico, in: Alteraciones y Paleoalteraciones en la morfología del oeste peninsular, edited by: Martín-Serrano, A., Molina Ballesteros, E., and Blanco, J. A., Instituto Geológico y Minero de España, Monografí a 4, 27–43, 1991.

Molina Ballesteros, E., Alonso Gavilán, G., and Garcí a Talegón, J.: Nuevas aportaciones al estudio del "siderolítico" (Fm. Areniscas de Salamanca), Borde Oeste de la Cuenca del Duero (Zamora), Geogaceta, 42, 27–30, 2007.

Orue-Etxebarria, X., Pujalte, V., Bernaola, G., Apellaniz, E., Baceta, J. I., Payros, A., Núñez-Betelu, K., Serra-Kiel, J., and Tosquella. J.: Did the Late Paleocene Thermal Maximum affect the evolution of larger foraminifers?: evidences from calcareous plankton of the Campo section (Pyrenees, Spain), Mar. Micropaleontol., 41, 45–71, 2001.

Orue-Etxebarria, X., Bernaola, G., Baceta, J. I., Angori, E., Caballero, F., Monechi, S., Pujalte, V., Dinarès-Turell, J., Apellaniz, E., and Payros, A.: New constraints on the evolution of planktic foraminifers and calcareous nannofossils across the Paleocene–Eocene boundary interval: the Zumaia section revisited, N. Jb. Geo. Palaont. Abh., 234, 223–259, 2004.

Plaziat, J. C.: Signification paléogéografique dex "calcaires conglomérés des brèches et des niveaux a rhodophycées" dans la sédimentation carbonatée du bassin Basco-Béarnais à la base du Tertiaire (Espagne-France), Rev. Géogr. Phys. Geol. Dyn., 17, 239–258, 1975.

Plaziat, J. C.: Late Cretaceous to late Eocene paleogeographic evolution of southwest Europe, Palaeogeogr. Palaeocl., 36, 263–320, 1981.

Plink-Björklund, P. and Steel, R. J.: Initiation of turbidity currents: outcrop evidence for Eocene hyperpycnal flow turbidite, Sedim. Geol., 165, 29–52, 2004.

Pujalte, V., Baceta, J. I., Payros, A., Orue-Etxebarria, X., and Serra-Kiel, J.: Late Cretaceous – Middle Eocene Sequence Stratigraphy and Biostratigraphy of the SW and W Pyrenees (Pamplona and Basque Basins): a Field Seminar of the Groupe de Etude du Paleogene and IGCP Project 286, Universidad del País Vasco/Euskal Herriko Univertsitatea, 118 pp., doi:10.13140/2.1.3746.6407, 1994.

Pujalte, V., Schmitz, B., Baceta, J. I., Orue-Etxebarria, X., Núñez-Betelu, K., Payros, A., and Serra-Kiel, J.: An early "Ilerdian" transient switch-off in shallow and deep-water carbonate

CPD
11, 2889–2931, 2015

deposition in the Western Pyrenees, Spain: origin and relevance for the Paleocene/Eocene boundary, Strata, 9, 111–112, 1998a.

Pujalte, V., Baceta, J. I., Orue-Etxebarria, X., and Payros, A.: Paleocene strata of the Basque Country, W Pyrenees, N Spain: facies and sequence development in a deep-water, starved basin, in: Mesozoic and Cenozoic Sequence Stratigraphy of European basins, edited by: de Graciansky, P. C., Hardenbol, J., Jacquin, T., and Vail, P. R., SEPM Special Publication, 60, 311–325, 1998b.

Pujalte, V., Orue-Etxebarria, X., Schmitz, B., Tosquella, J., Baceta, J. I., Payros, A., Bernaola, G., Caballero, F., and Apellaniz, E.: Basal Ilerdian (earliest Eocene) turnover of larger foraminifera: age constraints based on calcareous plankton and $\delta^{13}C$ isotopic profiles from new southern Pyrenean sections (Spain), in: Causes and Consequences of Globally Warm Climates in the Early Paleogene, edited by: Wing, S. L., Gingerich, P. D., Schmitz, B., and Thomas, E., Geological Society of America Special Paper 369, 205–221, 2003.

Pujalte, V., Schmitz, B., Baceta, J. I., Orue-Etxebarria, X., Bernaola, G., Dinarès-Turell, J., Payros, A., Apellaniz, E., and Caballero, F.: Correlation of the Thanetian-Ilerdian turnover of larger foraminifera and the Paleocene-Eocene Thermal Maximum: confirming evidence from the Campo area (Pyrenees, Spain), Geol. Acta, 7, 161–175, 2009.

Pujalte, V., Schmitz, B., and Baceta, J. I.: Sea-level changes across the Paleocene–Eocene interval in the Spanish Pyrenees, and their possible relationship with North Atlantic magmatism, Palaeogeogr. Palaeocl., 393, 45–60, 2014a.

Pujalte, V., Robador, A., Payros, A., and Samsó J. M.: Input of coarse-grained siliciclastics into the Pyrenean Basin during the PETM (2): a river-dominated fandelta within a carbonate platform system, Rendiconti Online Soc. Geol. It., 31, 179–180, 2014b.

Ríos Aragüés, L. M., Lanaja, J. M., and Frutos, E.: Mapa Geológico de España a escala 1 : 50.000, Hoja 178, Broto, Instituto Geológico y Minero de España, IGME, Madrid, 1972.

Santisteban Navarro, J. I., Martín-Serrano, A., Mediavilla, R., and Molina Ballesteros, E.: Introducción a la Estratigrafía de la Cuenca del Duero, in: Alteraciones y Paleoalteraciones en la morfología del oeste peninsular, edited by: Martín-Serrano, A., Molina Ballesteros, E., and Blanco, J. A., Instituto Geológico y Minero de España, Monografí a 4, 185–198, 1991.

Scheibner, C., Speijer, R. P., and Marzouk, A.: Larger foraminiferal turnover during the Paleocene/Eocene thermal maximum and paleoclimatic control on the evolution of platform ecosystems, Geology, 33, 493–496, 2005.

CPD
11, 2889–2931, 2015

Schmitz, B. and Pujalte, V.: Sea-level, humidity, and land-erosion records across the initial Eocene Thermal Maximum from a continental-marine transect in northern Spain, Geology, 31, 689–692, 2003.
Schmitz, B. and Pujalte, V.: Abrupt increase in seasonal extreme precipitation at the Paleocene-Eocene boundary, Geology, 35, 215–218, 2007.
Schmitz, B., Asaro, F., Molina, E., Monechi, S., Von Salis, K., and Speijer, R.: High-resolution iridium, d13C, d18O, foraminifera and nannofossil profiles across the latest Paleocene benthic extinction event at Zumaya, Palaeogeogr. Palaeocl., 133, 49–68, 1997.
Schmitz, B., Pujalte, V., and Núnez-Betelu, K.: Climate and sea-level perturbations during the Initial Eocene Thermal Maximum: evidence from siliciclastic units in the Basque Basin (Ermua, Zumaya and Trabakua Pass), northern Spain, Palaeogeogr. Palaeocl., 165, 299–320, 2001.
Schmitz, B., Pujalte, V., Molina, E., Monechi, S., Orue-Etxebarria, X., Speijer, R. P., Alegret, L., Apellaniz, E., Arenillas, I., Aubry, M.-P., Baceta, J.-I., Berggren, W. A., Bernaola, G., Caballero, F., Clemmensen, A., Dinarès-Turell, J., Dupuis, C., Heilmann-Clausen, C., Hilario Orus, A., Knox, R., Martin-Rubio, M., Ortiz, S., Payros, A., Petrizzo, M. R., von Salis, K., Sprong, J., Steurbaut, E., and Thomsen, E.: The global stratotype sections and points for the bases of the Selandian (Middle Paleocene) and Thanetian (Upper Paleocene) stages at Zumaia, Spain, Episodes, 34, 220–243, 2011.
Segura, M. and Elorza, J.: Presencia de ventifactos en las facies Utrillas (Tamajón-Sacedoncillo, borde Suroriental del Sistema Central, Guadalajara): aspectos morfológicos y procedencia, Revista de la Sociedad Geológica de España, 26, 47–63, 2013.
Serra-Kiel, J., Hottinger, L., Caus, E., Drobne, K., Ferrandez, C., Jauhri, A. K., Less, G., Pavlovec, R., Pignatti, J., Samso, J. M., Schaub, H., Sirel, E., Strougo, A., Tambareau, Y., Tosquella, J., and Zakrevskaya, E.: Larger foraminiferal biostratigraphy of the Tethyan Paleocene and Eocene, Bull. Soc. Geol. Fr., 169, 281–299, 1998.
Speijer, R. P. and Morsi, A. M. M.: Ostracode turnover and sea-level changes associated with the Paleocene-Eocene Thermal Maximum, Geology, 30, 23–26, 2002.
Strong, N. and Paola, C.: Valleys that never were: time surfaces versus stratigraphic surfaces, J. Sediment. Res., 78, 579–593, 2008.
Storme, J.-Y., Devleeschouwer, X., Schnyder, J., Cambier, G., Baceta, J. I., Pujalte, V., Di Matteo, A., Iacumin, P., and Yans, J.: The Palaeocene/Eocene boundary section at Zumaia (Basque-Cantabric Basin) revisited: new insights from high-resolution magnetic susceptibility

CPD
11, 2889–2931, 2015

and carbon isotope chemostratigraphy on organic matter ($d^{13}C_{org}$), Terra Nova, 24, 310–317, 2012.
Storme, J.-Y., Steurbaut, E., Devleeschouwer, X., Dupuis, C., Iacumin, P., Rochez, G., and Yans, J.: Integrated bio-chemostratigraphical correlations and climatic evolution across the Danian–Selandian boundary at low latitudes, Palaeogeogr. Palaeocl., 414, 212–224, 2014.
van Vliet, A.: Submarine Fans and Associated Deposits in the Lower Tertiary of Guipuzcoa (Northern Spain), PhD thesis, Lanbouwhogeschool Wageningen, the Netherlands, 45 pp., 1982.
Wade, B. S., Pearson, P. N., Berggren, W. A., and Pälike, H.: Review and revision of Cenozoic tropical planktonic foraminiferal biostratigraphy and calibration to the geomagnetic polarity and astronomical time scale, Earth-Sci. Rev., 104, 111–142, 2011.
Zamagni, J., Mutti, M., Ballato, P., and Kosir, A.: The Paleocene–Eocene thermal maximum (PETM) in shallow-marine successions of the Adriatic carbonate platform (SW Slovenia), Geol. Soc. Am. Bull., 124, 1071–1086, 2012.

CPD
11, 2889–2931, 2015

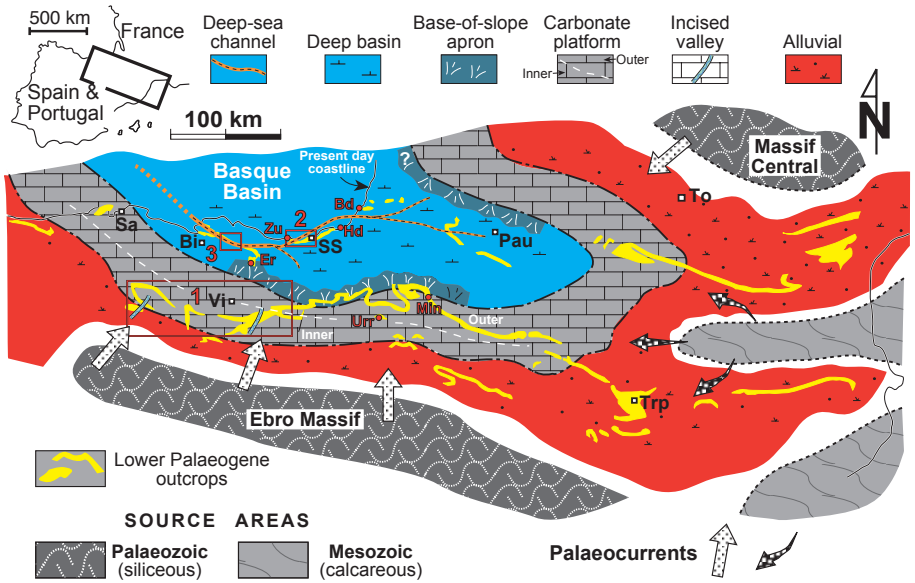

Figure 1. Early Palaeogene palaeogeography of the Pyrenean area, (modified from Baceta et al., 2004). The separation of inner and outer platform sub-domains (white broken line) is approximate. Boxes mark the location of study areas (1, incised valleys; 2 and 3 deep-sea channel deposits). Note the two different source areas, respectively supplying calciclastic and siliciclastic materials. Main cities: Bi, Bilbao; Pau; Sa, Santander; SS, San Sebastian; Trp, Tremp; Vi, Vitoria. Reference sections: Bd, Bidart; Er, Ermua; Hd, Hendaia; Mi, Mintxate; Ur, Urrobi; Zu, Zumaia.

CPD
11, 2889–2931, 2015

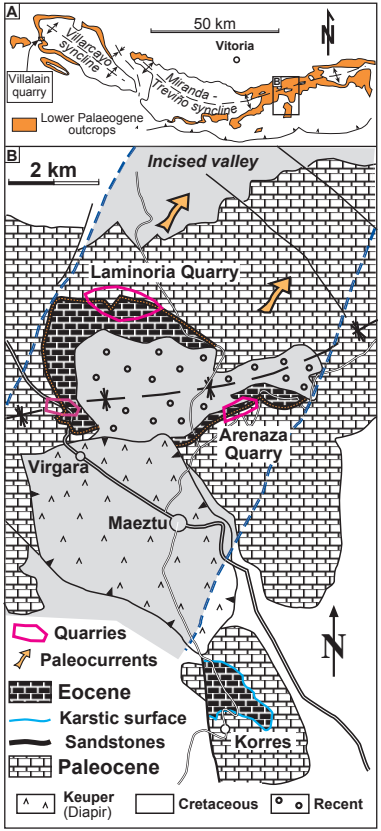

Figure 2. (a) Lower Palaeogene outcrops of the southwestern Pyreneees, with location of the Laminoria-Korres area and the Villalain quarry (see also Fig. 1). **(b)** Detailed outcrop map of the Laminoria-Korres area (location in box above), with interpretative plan view of the incised valley.

CPD
11, 2889–2931, 2015

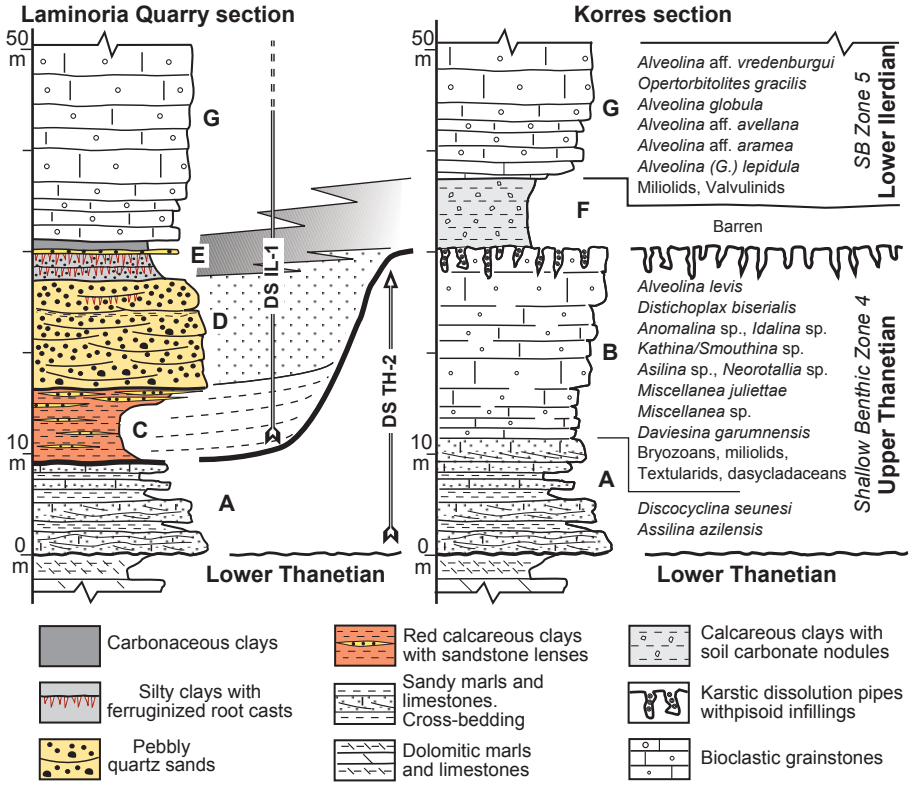

Figure 3. Columnar sections of the Laminoria Quarry and Korres sections across the Paleocene–Eocene interval. DS, Depositional sequences. A–G, lithological units described in the text.

CPD
11, 2889–2931, 2015

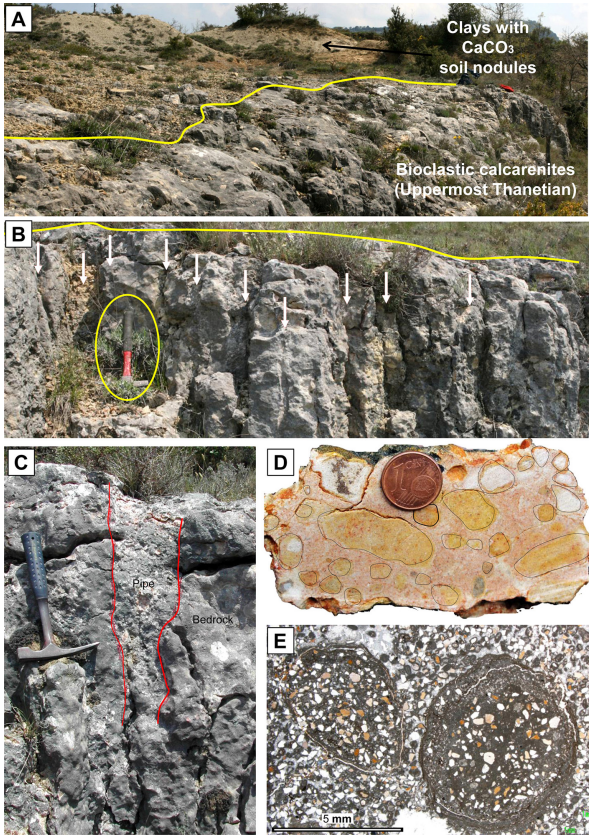

Figure 4. Field images of the Korres section. **(a)** General view of the irregular karstified surface capping the upper Thanetian marine carbonates of unit B. (**b** and **c**) Overview and close-up of the prominent vertical dissolution pipes of the top part of unit B. **(d)** Polished hand sample of the pisoid-bearing infilling of the dissolution pipes. **(e)** Microphotograph of pisoids.

CPD
11, 2889–2931, 2015

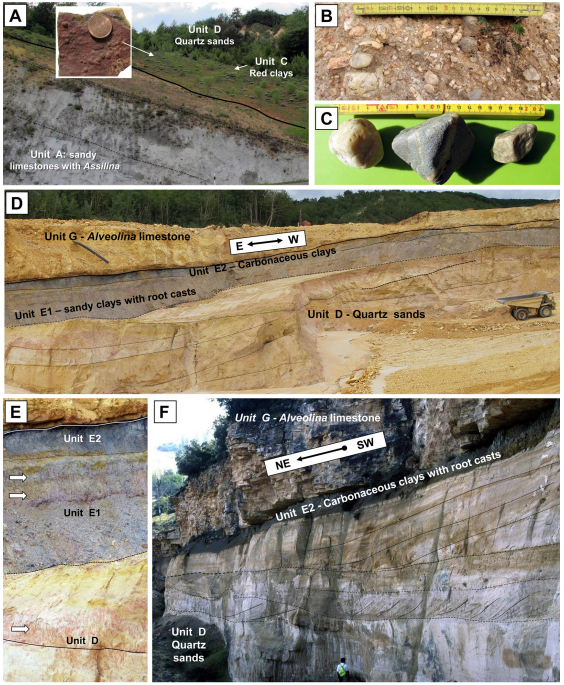

Figure 5. Incised valley deposits. **(a)** Abandonned quarry to the north of Virgara: general view of unit C (continental red clays with sandstone lenses) abruptly overlying upper Thanetian sandy marls and limestones of unit A. The inset illustrate the upper surface of a sandstone lens coated with goethite-hematite. **(b)** Close-up of a pebble-rich part of Unit D. **(c)** Examples of sub-rounded pebbles of unit D preserving flattened facets suggestive of ventifacts. **(d)** General view of units D–G in the active quarry front of Laminoria. Note concave-up internal erosional surfaces in unit D (quartz sands). The dumper is about 6.5 m high. **(e)** Close-up of a part of the Laminoria quarry, the white arrows indicating horizons with hematite-coated root casts. **(f)** Units D–G in the Villalain Quarry; note large-scale unidirectional cross-bedding in unit D.

CPD
11, 2889–2931, 2015

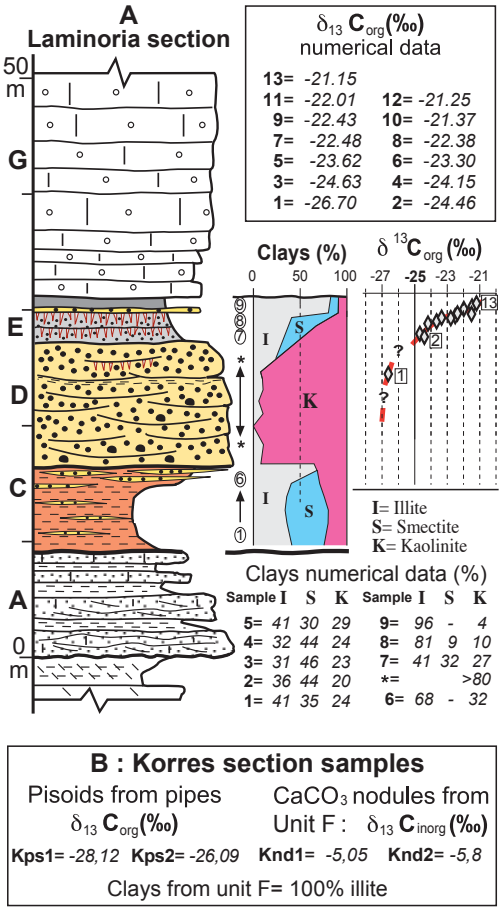

Figure 6. (a) Clay-mineral and stable isotope data from the Laminoria quarry section. **(b)** Clay-mineral and stable isotope data from the Korres section. Explanation within the text.

CPD
11, 2889–2931, 2015

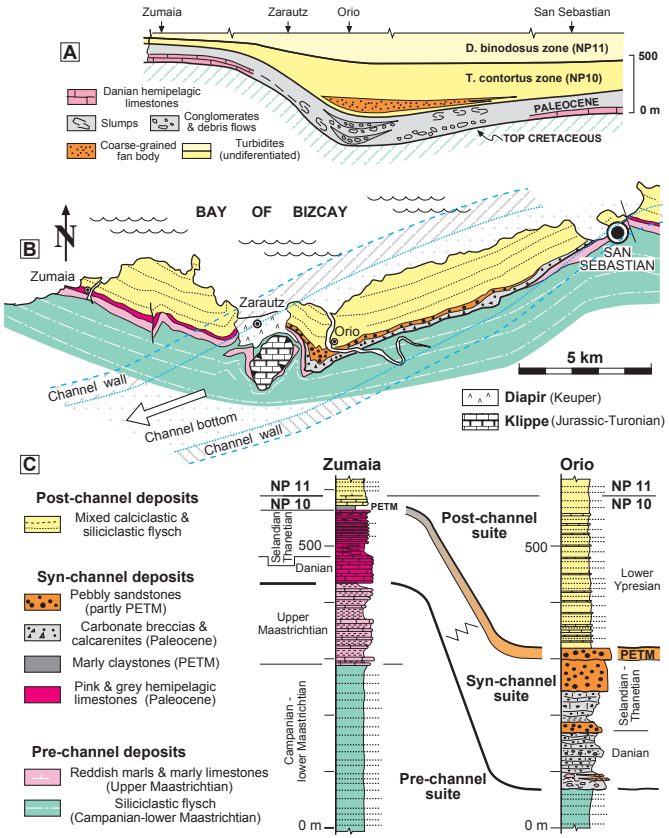

Figure 7. (a) Stratigraphic cross-section of the Zumaia-San Sebastian area, redrawn from Fig. 60 of van Vliet (1982). Note that the Cretaceous succession was undifferentiated. **(b)** Outcrop map with superimposed palaeogeography of a segment of the Paleocene deep-sea channel in the same area (location, box 2 in Fig. 1). **(c)** Correlation of the representative Orio and Zumaia sections using the NP10/NP11 boundary as datum. Explanation within the text.

CPD
11, 2889–2931, 2015

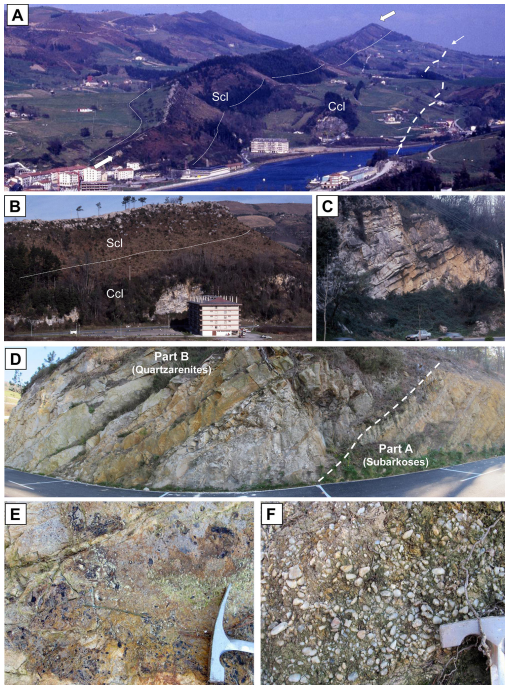

Figure 8. (a) General view of deep-sea channel deposits to the east of Orio (the village is situated in the bottom left hand corner of the image). The broken thick white line and the small white arrows indicate the base of the deep-sea channel succession, the big white arrows point to the prominent ridge created by the PETM quartzarenites; Ccl, part of the succession dominated by calciclastic deposits; Scl, part of the succession dominated by siliciclastic deposits. (**b** and **c**) General view and close up of Ccl deposits in quarries next to the N-634 road; **(d)** field view of upper part of the Scl-dominated succession, corresponding to the P–E interval, with indication of the two parts (**a** and **b**) differentiated. **(e)** Coal remains on the top surface of a quartzarenite bed from part B. **(f)** Close up of the pebbly quartzarenite at the lower part B.

CPD
11, 2889–2931, 2015

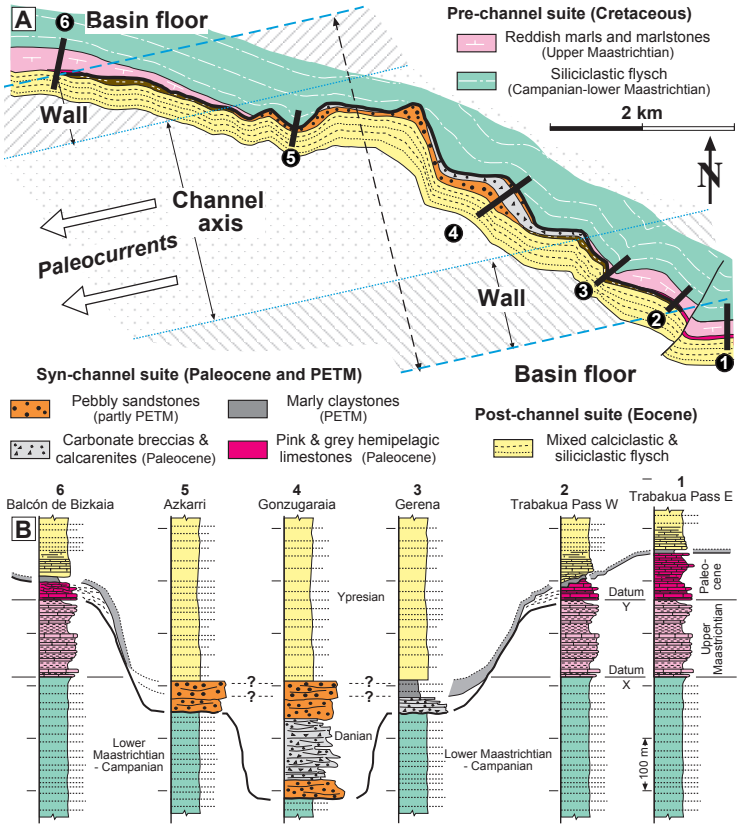

Figure 9. (a) Outcrop map, with superimposed palaeogeography, of the segment of the Paleocene deep-sea channel in the Gonzugaia-Trabakua pass area (location: box 2 in Fig. 1). **(b)** Correlation of representative sections using two datums: X, lower-upper Maastrichtian boundary; Y, Cretaceous-Palaeogene boundary. Note that PETM clays drape the channel walls (Trabakua W section) and cover the basin floor (Trabakua E section). Modified from Baceta (1996). Explanation within the text.

CPD
11, 2889–2931, 2015

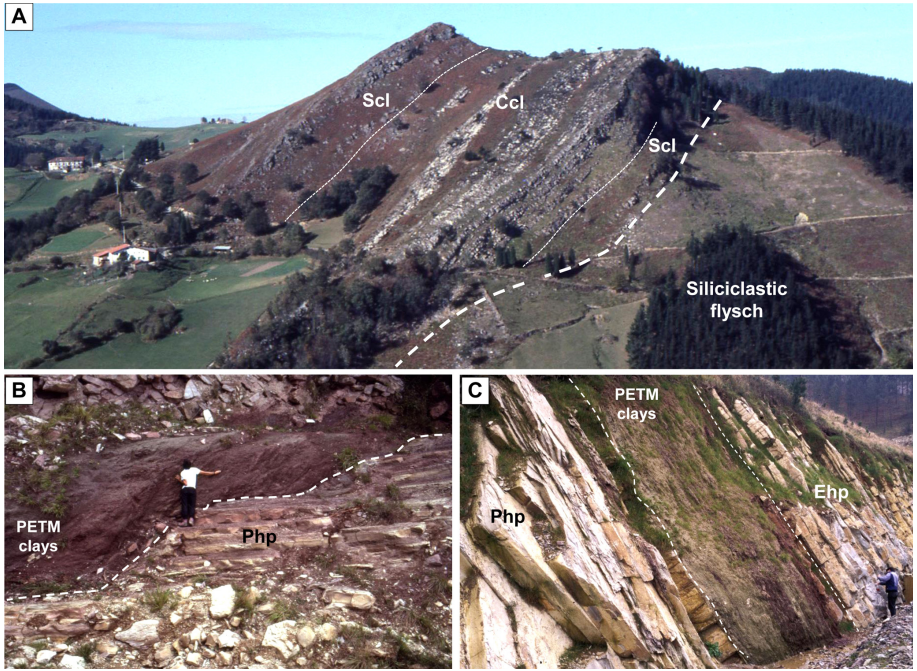

Figure 10. Field images of representative sections of the deep-sea channel in the Gonzugaraia-Trabakua pass area. **(a)** Gonzugaraia section; **(b)** Trabakua west section; **(c)** Trabakua east section (locations in Fig. 7). Scl: siliciclastic-dominated intervals; Ccl, claciclastic dominated intervals; Php, Paleocene hemipelagic deposits; Ehp, Eocene hemipelagic deposits.

CPD
11, 2889–2931, 2015

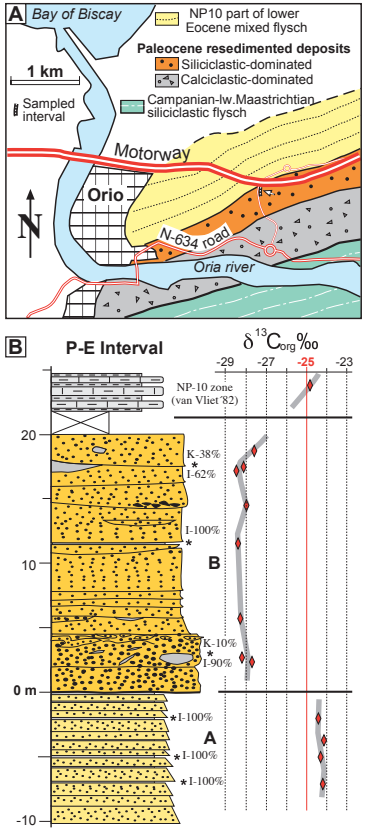

Figure 11. (a) Simplified geological map of a sector to the east of Orio, with location of the studies P–E interval (arrowed). **(b)** Columnar sections across the P–E interval of the Orio section and stable isotope profile of organic carbon. Asterisk indicate samples analyzed for clay minerals and their respective percentage.

CPD
11, 2889–2931, 2015

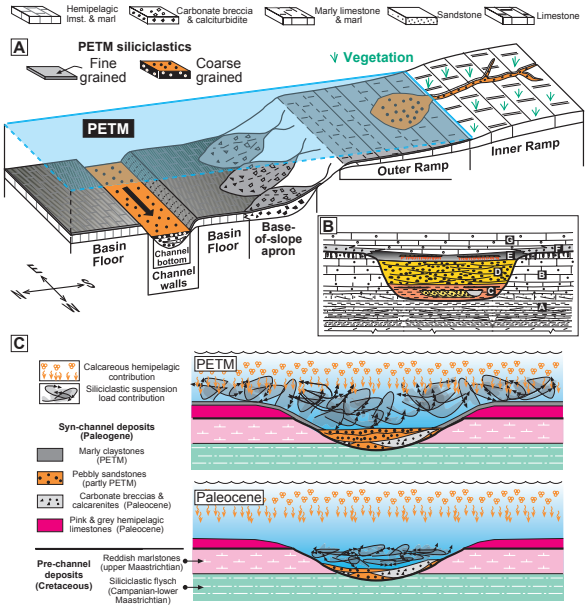

Figure 12. (a) Reconstructed S–N transects of the southwestern margin of Pyrenean Gulf during the PETM interval: coarse-grained sands and pebbly sands were accumulated within the incised valleys, deltas and within a deep-sea channel, while fine-grained siliciclastics mantled most other parts of the gulf. **(b)** Reconstructed architecture of the incised valleys. **(c)** Simplified graphic models depicting the depositional conditions in the Basque Basin during two different time intervals: during most of Paleocene times (lower image) clastic bed load and suspension load were largely confined to within the deep-sea channel, while hemipelagic deposition dominated on the basin floor; during the PETM (upper image), clastic input increased dramatically: coarse-grained bed-load remained confined to the deep-sea channel bottom, but suspension load became widespread over the entire basin, including the channel walls and the basin floor, diluting hemipelagic deposition.

CPD
11, 2889–2931, 2015